

MeSS: City Mesh-Guided Outdoor Scene Generation with Cross-View Consistent Diffusion

Xuyang Chen^{1,3}, Zhijun Zhai², Kaixuan Zhou³, Zengmao Wang³, Jianan He³, Dong Wang³, Yanfeng Zhang³, Mingwei Sun^{2,3}, Rüdiger Westermann¹, Konrad Schindler¹, Lirui Meng¹

¹TU Munich

²Wuhan University

³Huawei Riemann Lab

⁴ETH



Figure 1: Starting from textureless urban meshes, our MeSS synthesizes high-quality Gaussian Splatting Scenes with realistic appearance. After synthesis, these Gaussian scenes can be further rendered into stylized videos.

Abstract

Mesh models have become increasingly accessible for numerous cities; however, the lack of realistic textures restricts their application in virtual urban navigation and autonomous driving. To address this, this paper proposes MeSS (Mesh-based Scene Synthesis) for generating high-quality, style-consistent outdoor scenes with city mesh models serving as the geometric prior. While image and video diffusion models can leverage spatial layouts (such as depth maps or HD maps) as control conditions to generate street-level perspective views, they are not directly applicable to 3D scene generation. Video diffusion models excel at synthesizing consistent view sequences that depict scenes but often struggle to adhere to predefined camera paths or align accurately with rendered control videos. In contrast, image diffusion models, though unable to guarantee cross-view visual consistency, can produce more geometry-aligned results when combined with ControlNet. Building on this insight, our approach enhances image diffusion models by improving cross-view consistency. The pipeline comprises three key stages: first, we generate geometrically consistent sparse views using Cascaded Outpainting ControlNets; second, we propagate denser intermediate views via a component dubbed AGInpaint; and third, we globally eliminate visual inconsistencies (e.g., varying exposure) using the GCAlign module. Concurrently with generation, a 3D Gaussian Splatting (3DGS) scene is reconstructed by initializing Gaussian balls on the mesh surface. Our method outperforms existing approaches in both geometric alignment and generation quality. Once synthesized, the scene can be rendered in diverse styles through relighting and style transfer techniques.

1 Introduction

Projects like 3DCityDB (Yao, Chaturvedi, and Kolbe 2025), Hamburger LOD3 (Landesbetrieb Geoinformation und Vermessung Hamburg 2025), Ingolstadt LOD3 (SAVeNow 2020), and 3DBAG (Peters et al. 2022) provide detailed city-scale mesh models, typically at Level of Detail 3 (LoD3) for buildings. However, these models often lack high quality textures, relying instead on simple templates—or omitting textures entirely. This limitation hinders many downstream applications. For example, in VR-based urban navigation, texture quality is essential to user experience—especially at street level, where users are close enough to notice visual flaws.

While deploying data collection vehicles to gather additional street-view imagery may seem like a direct solution, it is prohibitively costly and still prone to issues such as occlusions and illumination variability. A more scalable and customizable alternative is to leverage generative models to enrich the visual appearance of mesh models. This approach is both cost-efficient and adaptable, enabling users to tailor scene aesthetics to their specific needs or preferences.

Recent works like (Chai et al. 2023; Lin et al. 2023; Chen, Wang, and Liu 2023; Xie et al. 2024a,b, 2025) have investigated to generate a city as NeRF (Mildenhall et al. 2021) or 3DGS (Kerbl et al. 2023) representations from city semantic & height map. Since their training process is supervised by images in birds-eye-view, their visual quality degrades significantly after zooming-in. This in turn has fueled efforts to synthetically generate visual data from the perspective on

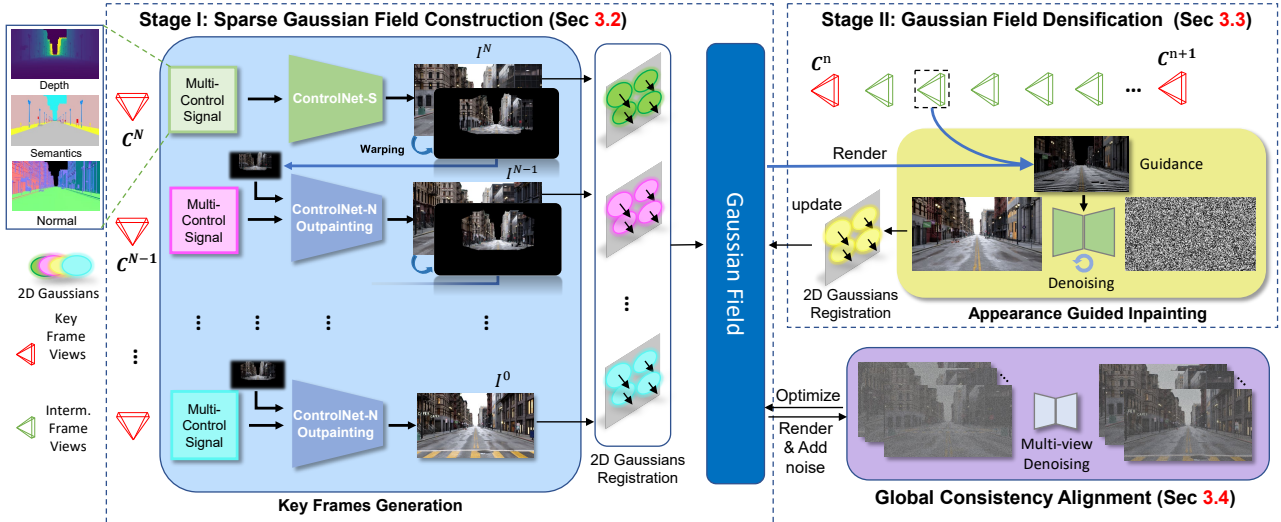


Figure 2: **Schematic illustration of MeSS.** Given a sequence of camera poses, we start by generating the last viewpoint using a *ControlNet-s*. Then we generate other key views in reverse order using a *ControlNet-n*, while transferring information backwards through the sequence. All generated pixels are projected onto the mesh surface as 2D Gaussian surfels. From the resulting Gaussian field, intermediate views are rendered and filled up with *Appearance-Guided Inpainting (AGInpaint)*, simultaneously densifying the Gaussian field. Each time the field is extended, a *Global Consistency Alignment* ensures spatial consistency by simultaneously denoising multi-view renderings.

the street.

To alleviate the cost and complexity of real-world data collection for autonomous driving, recent approaches (Wang et al. 2024b; Li, Zhang, and Ye 2024; Zhao et al. 2024a; Gao et al. 2025) have explored generating driving scenes directly from video diffusion models (Blattmann et al. 2023). These methods primarily focus on synthesizing foreground elements such as traffic participants and road infrastructure, leaving the background—particularly buildings—to be hallucinated by the generative model without explicit structural constraints. As a result, the generated videos often fail to align with the actual city layout or urban topology.

To tackle this limitation, Streetscapes (Deng et al. 2024) leverages simplified building geometries and map layouts as conditioning inputs to enhance geometric consistency. Similarly, Cosmos-Transfer1 (Alhaija et al. 2025) integrates background structures into the generation process by utilizing sparse depth data derived from lidar point clouds, though its depth control mechanism ignores all scene content beyond a 75-meter range. Nevertheless, due to the imprecise nature of their geometric inputs and the feedforward design of their conditional generation pipelines, these methods fail to guarantee precise geometric alignment.

Besides, video diffusion-based methods frequently suffer from temporal artifacts, manifesting as abrupt transitions or inconsistencies across frames. These limitations collectively highlight the necessity of constraining generation to adhere to actual mesh surfaces.

Directly texturing mesh models with 2D diffusion models (Chen et al. 2023a; Metzer et al. 2023; Chen et al. 2024; Richardson et al. 2023) may seem a viable option, but existing methods are limited to single objects or small scenes

with low polygon counts, far from city-scale street scenes. Another approach is perpetual view generation from a single image (Yu et al. 2024a,b; Wang et al. 2024a; Chung et al. 2023), which relies on progressively outpainting of RGB images and associated depth maps to cover the scene, using 2D diffusion models (Rombach et al. 2022). Their outpainting strategy often gradually drifts away from the initial appearance and is not capable for generating consistent dense views.

In summary, one must solve two main challenges to enable the scene generation with generative models: (i) Generate visual results aligning with given city surface models. (ii) Maintain a consistent appearance across long range without drifting.

We carefully design the MeSS pipeline to meet these requirements. A common approach for generating consecutive view sequences with 2D diffusion models is the *warp-and-outpaint* procedure, we optimize it by a two-staged framework. In Stage I, **Sparse key frames** are generated by two *Cascaded Outpainting ControlNets*, which consecutively outpaint new frames from preceding ones. With it, appearance drifts among key frames can be largely reduced in a long range. Meanwhile, All key frames are spread as Gaussian balls on the surface of mesh model to guarantee the geometry alignment. Sparse-view reconstructed Gaussian Scene commonly depicts blurry artifacts or silhouette in denser novel views. In Stage II, we fix these issues by optimizing the Gaussian Scene at these views.

To that end, we make the following technical contributions:

- We introduce **Cascaded Outpainting ControlNets** conditioned on preceding frame to generate consistent key

frames to ensure long range consistency.

- We devise a **Appearance Guided Inpainting** method to meticulously inpaint the occluded area in the intermediate dense views using the guidance of surrounding known regions.
- Our method achieves state-of-the-art (SOTA) performance in generating 3D Scene from city mesh models, ensuring high appearance fidelity and cross-view consistency.

2 Related Works

2.1 Scene Generation from 2D Map

InfiniCity (Lin et al. 2023) decomposes 3D scene generation into three steps: 2D map generation, map-to-voxel lifting, and voxel texturing through neural rendering. Scene-Dreamer (Chen, Wang, and Liu 2023) represents unbounded 3D landscapes via a bird’s-eye view (BEV) layout with height and semantic fields, manipulated through 2D generative models. Recent extensions like CityDreamer (Xie et al. 2024a) and its temporal variant CityDreamer4D (Xie et al. 2025) refine this paradigm by decomposing the rendering process into specialized modules for distinct scene components. CityDreamer4D explicitly separates static backgrounds, dynamic buildings, and movable foreground objects, while incorporating temporal consistency for 4D urban scene synthesis. Despite these advancements, existing methods (Xie et al. 2024b,a, 2025) still face challenges in stabilizing layout generation and achieving high-fidelity rendering.

2.2 Perpetual View Generation

Infinite-Nature (Liu et al. 2021) defines perpetual view generation as synthesizing views along arbitrary camera trajectories from a single image, employing a render-and-refine pipeline that progressively extends scenes via outpainting with cross-frame depth alignment. This principle has been extended through GANs (Li et al. 2022) and diffusion models: DiffDreamer (Cai et al. 2023) and SceneScape (Fridman et al. 2023) focus on static scene extrapolation, while WonderWorld (Yu et al. 2024a) enables interactive 3D scene generation through guided depth diffusion, allowing users to specify scene contents and viewpoints. For view-consistent generation, VistaDream (Wang et al. 2024a) explicitly enforces multiview geometry constraints during denoising process. These and other similar approaches (Chung et al. 2023; Yu et al. 2024b) all profit from advances in monocular depth estimation (Ranftl et al. 2020; Bhat et al. 2023; Ke et al. 2024a). However, they still exhibit rapid appearance drift in complex scenarios like urban driving, where error accumulation in the outpainting step amplifies inconsistencies across occluded regions.

2.3 Scene Synthesis from Video Generation

In the context of scene construction, video generators offer a way to synthesize (approximately) consistent views, either by conditioning on a single frame (Yu et al. 2024c; Fan et al. 2024; Sun et al. 2024) or by interpolating multiple given viewpoints (Liu et al. 2024; Yu et al. 2024c; Sun

et al. 2024). In particular, StreetScapes (Deng et al. 2024) addresses a task similar to ours with a two-frame video generator based on AnimateDiff (Guo et al. 2023a). Rendered depth, height, and semantics are used as control inputs to generate consecutive street views. Despite starting from a pretrained Latent Diffusion Model (Rombach et al. 2022), training such a video generator is expensive in terms of training data and compute. The insufficient geometric controlling ability also leads to adjacent-frame inconsistency and temporal drift in long sequence.

3 Methods

The MeSS pipeline (Fig. 2) is designed to synthetically generate viewpoints to reconstruct gaussian scene following a sparse-to-dense scheme. Given a 3D city map (i.e., a mesh model with semantic and instance labels but without texture), we specify a virtual camera path via a sequence of M views.

In **Stage I**, we generate a subset of N key view images along the sequence via a *warp-and-outpaint* procedure: starting from the initial key frame generated by geometric-conditioned *ControlNet-s*, each proceeding key frame is warped as an additional condition to the outpainting of new key frame with *ControlNet-n* (Sec. 3.2). After obtaining all key frames, we use them to construct a Gaussian field through optimizing gaussian surfels on the surface of mesh models.

In **Stage II**, we render from gaussian scene the intermediate views $\{\mathcal{C}^l\}, l \in \left(1, \frac{M}{N-1} - 2\right)$ between each pair of subsequent key views. Artifacts like silhouettes in intermediate frames are filled up by *Appearance Guided Inpainting* (Sec. 3.3). Lastly, *Global Consistency Alignment* (Sec. 3.4) further enhances the appearance consistency of gaussian surfels learned from different views.

3.1 Preliminaries

Latent Consistency Model. We utilize a *Latent Consistency Model* (LCM) to enhance the inpainting consistency across views in our method. Its core idea is to learn a function that maps any point on a trajectory of the *probability flow ODE* (Song et al. 2020; Lu et al. 2022) to that trajectory’s origin (i.e., the solution of the ODE). LCM is trained by enforcing the self-consistency property with a consistency function f_θ :

$$f_\theta(\mathbf{z}_t, \mathbf{c}, t) = f_\theta(\mathbf{z}_{t'}, \mathbf{c}, t'), \forall t, t' \in [\delta, T], \quad (1)$$

with δ a fixed, small positive number and T refers total diffusion steps. For ϵ -prediction (Song et al. 2020), the function f_θ is parameterized as

$$f_\theta(\mathbf{z}_t, \mathbf{c}, t) = c_{\text{skip}}(t)\mathbf{z}_t + c_{\text{out}}(t)\frac{(\mathbf{z}_t - \sigma(t)\hat{\epsilon}_\theta(\mathbf{z}_t, \mathbf{c}, t))}{\alpha(t)}, \quad (2)$$

where $c_{\text{skip}}(t)$ and $c_{\text{out}}(t)$ are scaling factors dependent on timestep t , and $\hat{\epsilon}_\theta(\mathbf{z}_t, \mathbf{c}, t)$ is the noise prediction model of LCM. During inference, the noise-free estimate $\tilde{\mathbf{z}}_0$ can be found as $\tilde{\mathbf{z}}_0 = f_\theta(\mathbf{z}_t, \mathbf{c}, t)$ with a single denoising step.

3.2 Stage I: Gaussian Field Construction from Key Views

Key Views Generation with Cascaded ControlNets. Two multi-conditioned *ControlNets* (Zhang, Rao, and Agrawala 2023) are introduced to generate N key views in autoregressive fashion, moving backwards from the end to the start of the camera path¹. First, *ControlNet-S* takes control signals $\{\mathbf{d}^N, \mathbf{s}^N, \mathbf{n}^N\}$ (depth, semantics and normals) at camera pose \mathcal{C}^N to generate view image \mathbf{I}^N . As single-channel disparity maps may lose the ability to discriminate depth values in the far field, so we encode depth as a colormap. This ensures depth variations are retained both near the camera and in the far field.

Having generated the last view image \mathbf{I}^N , we warp the image content to its previous key view \mathcal{C}^{N-1} via the known depth map. The reason for working backwards from the last frame is that, in a forward-facing camera, the warping will contract the pixel coordinates towards the image center. In this way, image generation artifacts due to limitations of the *ControlNet*, which mostly occur in the far field, will be diminished, whereas forward warping would amplify them and cause error build-up. To fill the peripheral regions where warped content is not available, *ControlNet-n* outpaints the missing values. On top of the inputs also used by *ControlNet-s* it takes the reference image $\tilde{\mathbf{I}}^{N-1}$ as additional condition to generate the final \mathbf{I}^{N-1} (See Appendix for more details). The alternation between warping and outpainting is repeated until the first view of the sequence is reached.

However, the extended key frames generated with the described *warp-and-outpaint* scheme may exhibit noticeable seams (Fig. 4b left) due to different exposures. To remove them and achieve coherent appearance, we synchronize all key frames with a *Global Consistency Alignment*, which will be discussed in Sec. 3.4).

Gaussian Field Construction On Mesh Surface From the set of keyframes $\{\mathbf{I}^n\}$, $n \in (0, N)$, a 3D Gaussian field is constructed. For the last frame \mathbf{I}^N (*i.e.* the first generated image) we instantiate a Gaussian splat for every pixel. In subsequent key frames \mathbf{I}^n , further Gaussians are added to fill in regions with low opacity values in the Gaussian field, in other words we also "outpaint" the Gaussians.

To avoid the computational cost associated with Gaussian Field optimization, splats are directly positioned on the known 3D surface by lifting image pixels according to the depth map. Furthermore, following the approach in SUGAR(Guédon and Lepetit 2024), the Gaussians are aligned with the surface and flattened by reducing the scale factor along the surface normal to a small value. The other two scale parameters are selected to ensure full coverage of the mesh surface, thereby preventing the formation of Moiré patterns and gaps (Yu et al. 2024a). For the Gaussians, Spherical Harmonics coefficients are computed from the RGB values of corresponding pixels, while opacity is set

based on empirical observations. Additional details are provided in the supplementary material.

3.3 Stage II: Gaussian Field Densification

Appearance Guided Inpainting We render from above constructed scene at intermediate novel views $\{\mathcal{C}^l\}$ between two keyframes \mathbf{I}^n and \mathbf{I}^{n+1} , $n \in [1, N]$. As illustrated in Fig. 3, the novel views are inspected with silhouettes since they are rendered from the coarse scene model. Novel views not included during the 3DGS reconstruction commonly suffer from holes and blurry textures (Kerbl et al. 2023). Inspired by (Epstein et al. 2023; Dhariwal and Nichol 2021; Luo et al. 2024; Yu et al. 2024a), we modify the sampling process of latent diffusion to obtain a training-free method for RGB inpainting, termed *Appearance Guided Inpainting* (AGInpaint). Specifically, AGInpaint rectifies the prediction



Figure 3: Silhouettes on novel views, marked with red ellipses and arrows.

of the score function ϵ_θ to the direction, that minimizes the discrepancy between diffusion prediction $\tilde{\mathbf{x}}_0$ ² and known RGB value \mathbf{x}_0 in the unmasked region \mathcal{M} . In simple words, the diffusion process should predict correct RGB values for known regions. This objective guides the diffusion model to predict aligned inpainting with neighbor pixels. At each sampling step, the rectification process is repeated N_g times, incrementally updating the latent with a low learning rate lr . This corresponds to a gradient descent towards a local optimum, thus preserving sharper details and more consistent texture within the reference image. The guided rectification is beneficial already in the initial stages of the sampling process: at earlier timesteps it aligns the overall color palette and dominant hues with those of the reference image, at later timesteps, the progressive refinement corrects fine-grained details and textures. For optimal performance of the guided inapinting we adopt LCM. Its self-consistency property Eq. (1) enables consistent estimation of the original sample \mathbf{x}_0 and stabilizes the guidance across different timesteps during diffusion sampling.

The complete process for guided inpainting is spelled out in Algorithm 1, where $\tilde{\mathbf{x}}_0$ is the noise-free one-step estimate of \mathbf{x}_t from the Consistency Function Eq. (2). \mathcal{M} denotes the unmasked region. To adaptively regulate the step size, we scale the gradients proportional to the mean absolute magnitude of the latent, respectively the gradients; thus accelerating convergence. The scaling is combined with the learning rate lr and denoted as s_t .

All newly inpainted pixels are spread onto the mesh surface in the aforementioned way.

¹Views are indexed in driving direction.

²By a slight abuse of notation, we skip the step from pixel space to latent space for simplicity.

Algorithm 1: Appearance Guided Sampling

```

1:  $\mathbf{x}_T \sim \mathcal{N}(\mathbf{0}, \mathbf{I})$ 
2: for  $t = T, \dots, 1$  do
3:    $\hat{\epsilon}_t^1 \leftarrow \epsilon_\theta(\mathbf{x}_t, c, t)$ 
4:   for  $n_g = 1, \dots, N_g$  do
5:      $\mathbf{g}_t = \nabla_{\mathbf{d}_t} \text{SmoothL1}(\tilde{\mathbf{x}}_0 \odot \mathcal{M}, \mathbf{x}_0 \odot \mathcal{M})$ 
6:      $s_t = lr \times \frac{\text{mean}(\hat{\epsilon}_t^{n_g})}{\text{mean}(|\mathbf{g}_t|)}$ 
7:      $\hat{\epsilon}_t^{n_g+1} = \hat{\epsilon}_t^{n_g} + s_t \mathbf{g}_t$ 
8:   end for
9:    $\mathbf{x}_{t-1} = \frac{1}{\sqrt{\alpha_t}} \left( \mathbf{x}_t - \frac{1-\alpha_t}{\sqrt{1-\alpha_t}} \hat{\epsilon}_t^{N_g} \right)$ 
10: end for
11: return  $\mathbf{x}_0$ 

```

3.4 Global Consistency Alignment

Gaussian field generated with the above two stages so far still exhibit appearance artifacts such as brightness drift, out-painting mistakes, etc. To resolve those, we draw inspiration from *Multiview Consistency Sampling* (MCS) in VistaDream (Wang et al. 2024a) and design a cleaning method called *Global Consistency Alignment* (GCA), tailored for our sparse-to-dense generation pipeline.

After the gaussian field construction process detailed in Sec. 3.2, we rerender a sequence of images $\mathbf{x}^{(1:N)}$ at the same camera viewpoints $\mathcal{C}^{(1:N)}$. We then apply the forward diffusion process to obtain $\mathbf{x}_T^{(1:N)}$ by adding T_1 steps of noise to $\mathbf{x}^{(1:N)}$. Using a learned LCM, we then derive a batch of noise-free estimates $\tilde{\mathbf{x}}_0^{(1:N)}$ through Eq. (2) and adjust it to $\bar{\mathbf{x}}_t^{(1:N)}$ via

$$\bar{\mathbf{x}}_t^{(n)} = w_t \gamma_t^{(n)} \mathbf{x}_t'^{(n)} + (1 - w_t) \tilde{\mathbf{x}}_0^{(n)}, n \in (1, N) \quad (3)$$

where $\gamma_t^{(n)} = \text{std}(\tilde{\mathbf{x}}_0^{(n)}) / \text{std}(\mathbf{x}_t'^{(n)})$ balances the exposure and w_t is a weight that governs the trade-off between the rendered $\mathbf{x}_t'^{(n)}$ and the $\tilde{\mathbf{x}}_0^{(n)}$ estimated by multi-view consistent denoising.

Next, the adjusted estimates $\bar{\mathbf{x}}_t^{(1:N)}$ serve to refine the Gaussian field, while $\mathbf{x}_t'^{(1:N)}$ are rendered from the updated scene after each refinement step. Here, $\bar{\mathbf{x}}_t^{(1:N)}$ achieves a balance between $\mathbf{x}_t'^{(1:N)}$ and $\tilde{\mathbf{x}}_0^{(1:N)}$, thus ensuring multi-view consistency while at the same time enhancing details through reverse diffusion.

Finally, the same method is used to also improve the consistency of views $\mathcal{C}^{(n:(n+1)k)}$, i.e., the sub-sequence of intermediate frames between (and including) two consecutive keyframes.

4 Experiments

4.1 Data Preparation and Implementation

To assess the feasibility of our pipeline, we render RGB images with corresponding depth, normal, and semantic maps using City Sample Project (Epic Games 2022) in Unreal Engine 5 (Epic Games 2021). ControlNets are trained upon frozen Stable Diffusion 1.5 (SD1.5) with training data rendered above. More details about data preparation and implementation can be found in the supplementary material.

Our pipeline is designed to address the challenge of scene generation on a predefined city mesh layout using image diffusion model. We compare our approach with other methods in the domains of 3D city generation, scene generation based on video synthesis, and perpetual view generation. For quantitative evaluation of the generated results, we employ the Fréchet Inception Distance (FID) and Kernel Inception Distance (KID) metrics. These metrics measure the discrepancy between the distributions of the generated results and the ground truth imagery, providing a standard benchmark for assessing the performance of generative models. To evaluate the consistency across views, we calculate the Learned Perceptual Image Patch Similarity (LPIPS) for extended views generated from a real image, offering insights into the perceptual quality and coherence of the synthesized sequences



Figure 4: a) The comparison result of Resample(left) vs. AGInpaint(right). AGInpaint performs better than Resample in slim region inpainting b) The comparison of results w/o(left) and w/(right) GCAAlign. GCAAlign is able to harmonize the seams brought by different exposures

4.2 Comparison with other methods

Baselines. Both WonderWorld (Yu et al. 2024a) and VistaDream (Wang et al. 2024a) rely on monocular depth estimation methods (Bochkovskii et al. 2024; Ke et al. 2024b) to give depth value for placing Gaussians into 3D space, while our method is based on mesh geometry with precise metric depth. To form a fair comparison, we inject metric depth into their pipelines and align their inpainting diffusion model with ours. The altered ones are named as WonderWorld[†] and VistaDream[†] respectively. For each camera path, We start the scene from the same initial view and outpaint them by moving the camera backwards for 100 meters using the two and our pipeline. In this way, 3200 images are produced in total.

As depicted in Tab. 1, our method achieves better metrics. We visualize several intermediate frames in Fig. 5 and observe that for the same outpainting task, we produce more consistent results aligning well with the underlining geometry, while they suffer a lot from quality degeneration caused by discrepancy accumulation of inpainting results. Even equipped with Multiview Consistency Sampling (Sec3.2 in VistaDream), VistaDream[†] does not show apparent improvement wrt. WonderWorld[†], which emphasizes the synchronisation of Multiview Consistency Alignment with consistent inpainting, as ours.

Comparison with Perpetual View Generation We also visualize the result of the naive Wonderworld in Fig. 5.

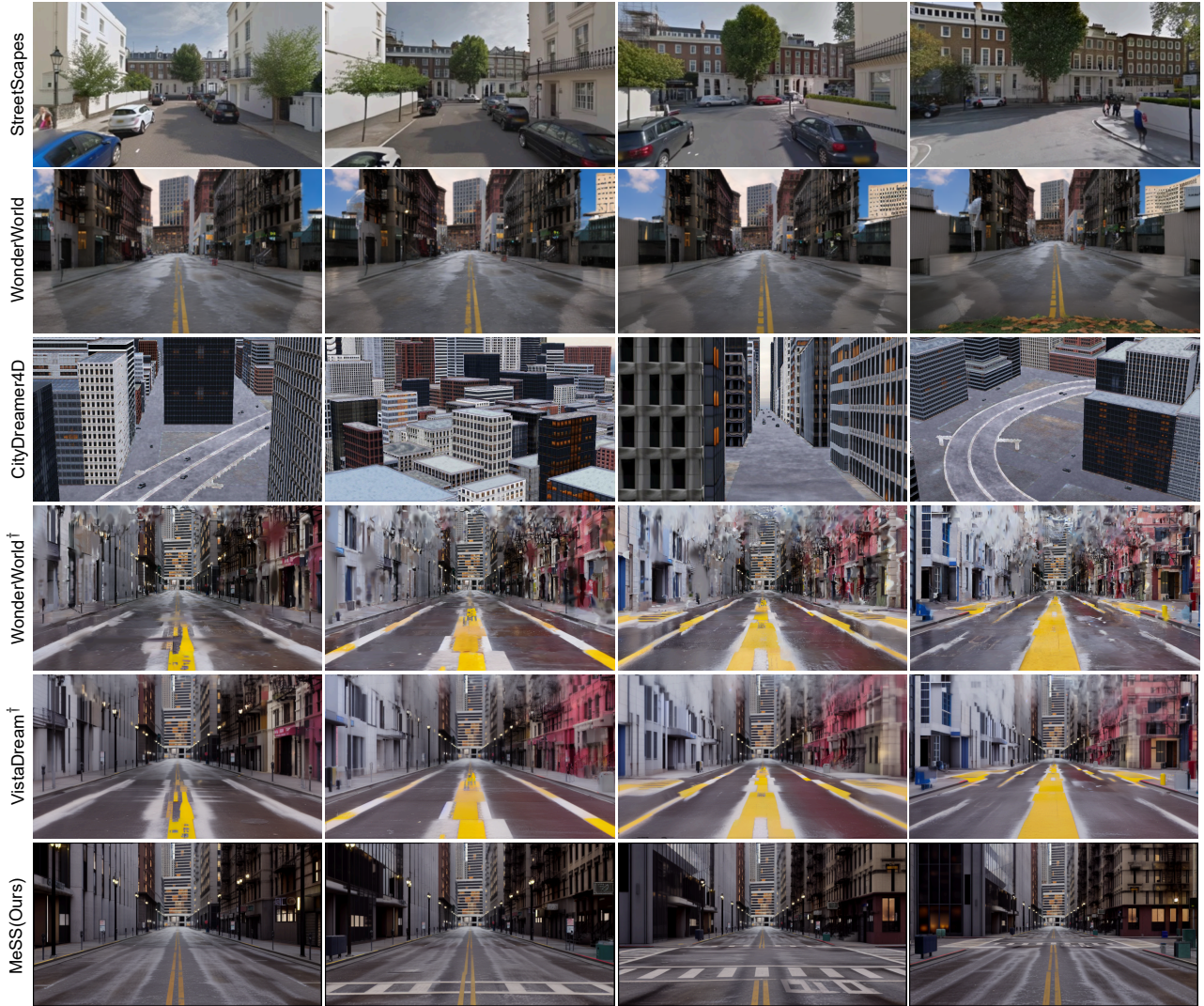


Figure 5: Visual comparison with other methods. Since there is no code provided by CityDreamer4D and Streetscapes, we take the visual results from their papers. Please zoom in to check for details.

Without any prior information about the building geometry it cannot extend their facades and the outpainted content is tending to be more irrelevant to the initial view. This verifies the difficulties of their method on this task.

Comparison with 3D City Generation CityDreamer4D (Xie et al. 2025) is implemented on the Citytopia dataset (Xie et al. 2025), which is also constructed based on the City Sample Project in Unreal Engine 5 (UE5), similar to ours. In comparison, our method demonstrates superior performance, as evidenced by lower scores in the FID and KID metrics. Furthermore, as illustrated in Fig. 5, their generated scenes exhibit notable limitations in visual quality upon closer inspection, particularly at street level. Specifically, the results lack critical urban elements such as streetlamps, traffic signs, and other street-level instances, significantly diminishing their realism and practical applicability.

Comparison with Video-Based Generation For StreetScapes (Deng et al. 2024), we directly use the results reported in their paper since their code is not publicly available. However, forming a fair comparison is challenging, as their model is trained on a significantly larger dataset compared to ours³. Given that our generated sequence is longer than theirs (200 frames vs. 64 frames), we evaluate their results within the range of 32 to 64 frames. In terms of quality, our results are on par with theirs, while we outperform them in terms of temporal consistency. This advantage can be attributed to our method’s effective utilization of geometric priors, which plays a key role in achieving superior consistency.

³Even for their experiment on the London patch, they utilize approximately 20 times more data than we do.

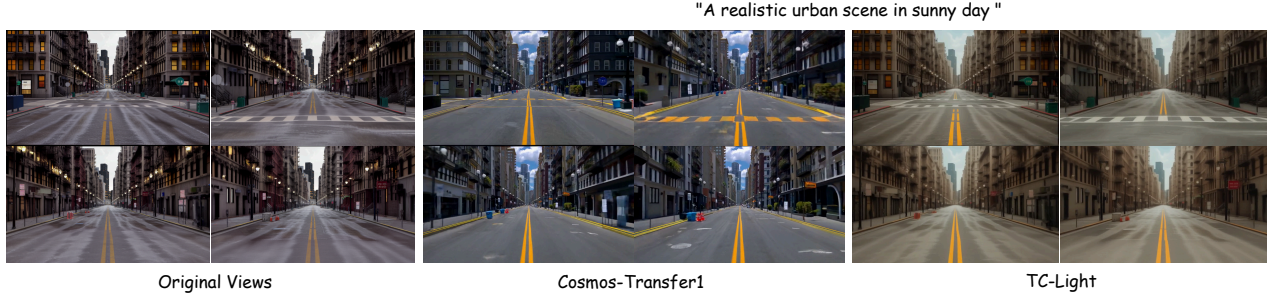


Figure 6: Stylized rendering results with Cosmos-Transfer1 and TC-Light. Please zoom in to check for details.

4.3 Stylized rendering

As you can see, the appearance of our generated scene is heavily branded with City Sample style, simply tweaking text prompt during view generation does not work for stylization. This hinders the application of the scene, so we develop a way to customize it through stylized rendering. Given a camera path in the scene, we render video and transfer it to different style via video relighting method TC-Light (Liu et al. 2025) or SDEdit (Meng et al. 2021) with Cosmos-Transfer1 (Alhaija et al. 2025). As depicted in Fig. 6, both are capable of completing this task by taking the original views as prior, and Cosmos-Transfer1 outperforms TC-Light in visual fidelity. The styled videos can be projected back to the gaussian scene if desired.

	LPIPS \downarrow	FID \downarrow	KID \downarrow
Citydreamer4D (Wang et al. 2024a)	-	88.48	0.049
WonderWorld-Geometry (Wang et al. 2024a)	0.516	75.807	0.076
Vistadream-Geometry (Yu et al. 2024a)	0.508	72.44	0.073
StreetScapes (Deng et al. 2024)	0.519	29.93	0.025
MeSS(Ours)	0.348	28.17	0.0161

Table 1: Quantitative evaluations on generated sequences

4.4 Ablation Study

Cascaded ControlNets For the outpainting task of key views in **Stage I**, we replace the preceding frame conditioned *ControlNet-N* by *ControlNet-S*. To make it different w.r.t. common warp-and-outpaint pipeline (Yu et al. 2024a,b), *AGInpaint* is still equipped. As depicted in Tab. 2, the fidelity of generated frames degenerates dramatically. Besides, the consistency is also getting worse due to larger appearance drift accumulated during scene extrapolation.

Appearance Guided Inpainting We replace the *AGInpaint* component in our method with a simpler approach called *Resample* (Deng et al. 2024; Lugmayr et al. 2022), which involves re-adding several rounds of noise at each denoising step to achieve a more homogeneous inpainted result. As demonstrated in Tab. 2, the absence of *AGInpaint* significantly impacts the generation quality. Through a visual comparison of the inpainted regions produced by *AGInpaint* and *Resample* (Fig. 4a), we highlight the superior

efficacy of *AGInpaint*. Due to the downsampling of inpainting masks, *Resample* struggles to fill in slim regions with Latent Diffusion Models, causing noticeable streak patterns.

ControlNet-n	AGInpaint	GCAlign	LPIPS	FID	KID
\times			0.382	54.54	0.0526
	\times		0.422	51.12	0.0459
		\times	0.346	26.25	0.0132

Table 2: Ablation studies on different components. \times means corresponding component is turned off.

Global Consistency Alignment As shown in the top portion of Fig. 4b, there is a noticeable lighting misalignment in the generated scene when *GCAlign* is not applied. However, after integrating *GCAlign* into our pipeline, the seams are effectively harmonized, as demonstrated in the bottom portion of Fig. 4b. An interesting observation is that *GCAlign* has a trade-off: while it improves visual coherence, it tends to introduce a slight blurring effect, leading to a loss of fine details. This is also reflected in the lower FID/KID metrics. Nevertheless, we consider this trade-off acceptable in favor of achieving a more visually consistent appearance.

5 Conclusion

In this paper, we present a pipeline for generating gaussian field from city surface models. Our method leverages a meticulously designed outpainting procedure, which ensures strong alignment with predefined scene geometry. Additionally, even after extensive view extrapolation, the newly generated regions maintain a coherent appearance with the preceding frames. This approach offers the advantage of low training costs and paves the way for utilizing real-world city 3D maps to synthesize Gausisan scenes.

6 Future Works

In future, we expect to integrate more advanced base models such as FLUX.1 or SD3, then anticipate significant improvements in resolution and overall quality. Additionally, we plan to explore the integration of geometric information into video diffusion, enhancing applicability for scene generation.

References

Alhaija, H. A.; Alvarez, J.; Bala, M.; Cai, T.; Cao, T.; Cha, L.; Chen, J.; Chen, M.; Ferroni, F.; Fidler, S.; et al. 2025. Cosmos-transfer1: Conditional world generation with adaptive multimodal control. *arXiv preprint arXiv:2503.14492*.

Bhat, S. F.; Birk, R.; Wofk, D.; Wonka, P.; and Müller, M. 2023. Zoedepth: Zero-shot transfer by combining relative and metric depth. *arXiv preprint arXiv:2302.12288*.

Blattmann, A.; Dockhorn, T.; Kulal, S.; Mendelevitch, D.; Kilian, M.; Lorenz, D.; Levi, Y.; English, Z.; Voleti, V.; Letts, A.; et al. 2023. Stable video diffusion: Scaling latent video diffusion models to large datasets. *arXiv preprint arXiv:2311.15127*.

Bochkovskii, A.; Delaunoy, A.; Germain, H.; Santos, M.; Zhou, Y.; Richter, S. R.; and Koltun, V. 2024. Depth pro: Sharp monocular metric depth in less than a second. *arXiv preprint arXiv:2410.02073*.

Cai, S.; Chan, E. R.; Peng, S.; Shahbazi, M.; Obukhov, A.; Van Gool, L.; and Wetzstein, G. 2023. Diffdreamer: Towards consistent unsupervised single-view scene extrapolation with conditional diffusion models. In *Proceedings of the IEEE/CVF International Conference on Computer Vision*, 2139–2150.

Chai, L.; Tucker, R.; Li, Z.; Isola, P.; and Snavely, N. 2023. Persistent nature: A generative model of unbounded 3d worlds. In *Proceedings of the IEEE/CVF conference on computer vision and pattern recognition*, 20863–20874.

Chen, D. Z.; Li, H.; Lee, H.-Y.; Tulyakov, S.; and Nießner, M. 2024. Scenetex: High-quality texture synthesis for indoor scenes via diffusion priors. In *Proceedings of the IEEE/CVF Conference on Computer Vision and Pattern Recognition*, 21081–21091.

Chen, D. Z.; Siddiqui, Y.; Lee, H.-Y.; Tulyakov, S.; and Nießner, M. 2023a. Text2tex: Text-driven texture synthesis via diffusion models. In *Proceedings of the IEEE/CVF International Conference on Computer Vision*, 18558–18568.

Chen, R.; Chen, Y.; Jiao, N.; and Jia, K. 2023b. Fantasia3d: Disentangling geometry and appearance for high-quality text-to-3d content creation. In *Proceedings of the IEEE/CVF international conference on computer vision*, 22246–22256.

Chen, Z.; Wang, G.; and Liu, Z. 2023. Scenedreamer: Unbounded 3d scene generation from 2d image collections. *IEEE transactions on pattern analysis and machine intelligence*.

Chung, J.; Lee, S.; Nam, H.; Lee, J.; and Lee, K. M. 2023. Luciddreamer: Domain-free generation of 3d gaussian splatting scenes. *arXiv preprint arXiv:2311.13384*.

Deitke, M.; Schwenk, D.; Salvador, J.; Weihs, L.; Michel, O.; VanderBilt, E.; Schmidt, L.; Ehsani, K.; Kembhavi, A.; and Farhadi, A. 2023. Objaverse: A universe of annotated 3d objects. In *Proceedings of the IEEE/CVF conference on computer vision and pattern recognition*, 13142–13153.

Deng, B.; Tucker, R.; Li, Z.; Guibas, L.; Snavely, N.; and Wetzstein, G. 2024. Streetscapes: Large-scale consistent street view generation using autoregressive video diffusion. In *ACM SIGGRAPH 2024 Conference Papers*, 1–11.

Dhariwal, P.; and Nichol, A. 2021. Diffusion models beat gans on image synthesis. *Advances in neural information processing systems*, 34: 8780–8794.

Epic Games. 2021. Unreal Engine 5. <https://www.unrealengine.com/en-US/unreal-engine-5>. Accessed: 2025-08-01.

Epic Games. 2022. City Sample Project. <https://www.unrealengine.com/marketplace/en-US/product/city-sample>. Accessed: 2025-08-01.

Epstein, D.; Jabri, A.; Poole, B.; Efros, A.; and Holynski, A. 2023. Diffusion self-guidance for controllable image generation. *Advances in Neural Information Processing Systems*, 36: 16222–16239.

Fan, Z.; Wen, K.; Cong, W.; Wang, K.; Zhang, J.; Ding, X.; Xu, D.; Ivanovic, B.; Pavone, M.; Pavlakos, G.; et al. 2024. InstantSplat: Sparse-view SfM-free Gaussian Splatting in Seconds. *arXiv preprint arXiv:2403.20309*.

Fridman, R.; Abecasis, A.; Kasten, Y.; and Dekel, T. 2023. Scenescape: Text-driven consistent scene generation. *Advances in Neural Information Processing Systems*, 36: 39897–39914.

Gao, S.; Yang, J.; Chen, L.; Chitta, K.; Qiu, Y.; Geiger, A.; Zhang, J.; and Li, H. 2025. Vista: A generalizable driving world model with high fidelity and versatile controllability. *Advances in Neural Information Processing Systems*, 37: 91560–91596.

Garland, M.; and Heckbert, P. S. 1997. Surface simplification using quadric error metrics. In *Proceedings of the 24th annual conference on Computer graphics and interactive techniques*, 209–216.

Guédon, A.; and Lepetit, V. 2024. Sugar: Surface-aligned gaussian splatting for efficient 3d mesh reconstruction and high-quality mesh rendering. In *Proceedings of the IEEE/CVF Conference on Computer Vision and Pattern Recognition*, 5354–5363.

Guo, Y.; Yang, C.; Rao, A.; Liang, Z.; Wang, Y.; Qiao, Y.; Agrawala, M.; Lin, D.; and Dai, B. 2023a. Animatediff: Animate your personalized text-to-image diffusion models without specific tuning. *arXiv preprint arXiv:2307.04725*.

Guo, Y.; Zuo, X.; Dai, P.; Lu, J.; Wu, X.; Yan, Y.; Xu, S.; Wu, X.; et al. 2023b. Decorate3d: text-driven high-quality texture generation for mesh decoration in the wild. *Advances in Neural Information Processing Systems*, 36: 36664–36676.

Ke, B.; Obukhov, A.; Huang, S.; Metzger, N.; Daudt, R. C.; and Schindler, K. 2024a. Repurposing diffusion-based image generators for monocular depth estimation. In *Proceedings of the IEEE/CVF Conference on Computer Vision and Pattern Recognition*, 9492–9502.

Ke, B.; Obukhov, A.; Huang, S.; Metzger, N.; Daudt, R. C.; and Schindler, K. 2024b. Repurposing Diffusion-Based Image Generators for Monocular Depth Estimation. In *Proceedings of the IEEE/CVF Conference on Computer Vision and Pattern Recognition (CVPR)*.

Kerbl, B.; Kopanas, G.; Leimkühler, T.; and Drettakis, G. 2023. 3d gaussian splatting for real-time radiance field rendering. *ACM Trans. Graph.*, 42(4): 139–1.

Landesbetrieb Geoinformation und Vermessung Hamburg. 2025. 3D-Gebäudemodell Lod3.0-HH. <https://metaver.de/trefferanzeige?docuqid=B438AD57-223B-43A4-8E74-767CEC8A96D7>. CityGML dataset, Freie und Hansestadt Hamburg, Datenlizenz Deutschland – Namensnennung 2.0. Last updated April 2025.

Li, X.; Zhang, Y.; and Ye, X. 2024. DrivingDiffusion: Layout-Guided Multi-view Driving Scenarios Video Generation with Latent Diffusion Model. In *European Conference on Computer Vision*, 469–485. Springer.

Li, Y.; Jiang, L.; Xu, L.; Xiangli, Y.; Wang, Z.; Lin, D.; and Dai, B. 2023. Matrixcity: A large-scale city dataset for city-scale neural rendering and beyond. In *Proceedings of the IEEE/CVF International Conference on Computer Vision*, 3205–3215.

Li, Z.; Wang, Q.; Snavely, N.; and Kanazawa, A. 2022. Infinitenature-zero: Learning perpetual view generation of natural scenes from single images. In *European Conference on Computer Vision*, 515–534. Springer.

Lin, C. H.; Lee, H.-Y.; Menapace, W.; Chai, M.; Siarohin, A.; Yang, M.-H.; and Tulyakov, S. 2023. Infinicity: Infinite-scale city synthesis. In *Proceedings of the IEEE/CVF International Conference on Computer Vision*, 22808–22818.

Liu, A.; Tucker, R.; Jampani, V.; Makadia, A.; Snavely, N.; and Kanazawa, A. 2021. Infinite nature: Perpetual view generation of natural scenes from a single image. In *Proceedings of the IEEE/CVF International Conference on Computer Vision*, 14458–14467.

Liu, F.; Sun, W.; Wang, H.; Wang, Y.; Sun, H.; Ye, J.; Zhang, J.; and Duan, Y. 2024. Reconx: Reconstruct any scene from sparse views with video diffusion model. *arXiv preprint arXiv:2408.16767*.

Liu, Y.; Luo, C.; Tang, Z.; Li, Y.; Yang, Y.; Ning, Y.; Fan, L.; Zhang, Z.; and Peng, J. 2025. TC-Light: Temporally Coherent Generative Rendering for Realistic World Transfer. *CoRR*.

Lu, C.; Zhou, Y.; Bao, F.; Chen, J.; Li, C.; and Zhu, J. 2022. Dpm-solver: A fast ode solver for diffusion probabilistic model sampling in around 10 steps. *Advances in Neural Information Processing Systems*, 35: 5775–5787.

Lugmayr, A.; Danelljan, M.; Romero, A.; Yu, F.; Timofte, R.; and Van Gool, L. 2022. Repaint: Inpainting using denoising diffusion probabilistic models. In *Proceedings of the IEEE/CVF conference on computer vision and pattern recognition*, 11461–11471.

Luo, G.; Darrell, T.; Wang, O.; Goldman, D. B.; and Holynski, A. 2024. Readout guidance: Learning control from diffusion features. In *Proceedings of the IEEE/CVF Conference on Computer Vision and Pattern Recognition*, 8217–8227.

Luo, S.; Tan, Y.; Huang, L.; Li, J.; and Zhao, H. 2023. Latent consistency models: Synthesizing high-resolution images with few-step inference. *arXiv preprint arXiv:2310.04378*.

Meng, C.; He, Y.; Song, Y.; Song, J.; Wu, J.; Zhu, J.-Y.; and Ermon, S. 2021. Sdedit: Guided image synthesis and editing with stochastic differential equations. *arXiv preprint arXiv:2108.01073*.

Metzer, G.; Richardson, E.; Patashnik, O.; Giryes, R.; and Cohen-Or, D. 2023. Latent-nerf for shape-guided generation of 3d shapes and textures. In *Proceedings of the IEEE/CVF Conference on Computer Vision and Pattern Recognition*, 12663–12673.

Mildenhall, B.; Srinivasan, P. P.; Tancik, M.; Barron, J. T.; Ramamoorthi, R.; and Ng, R. 2021. Nerf: Representing scenes as neural radiance fields for view synthesis. *Communications of the ACM*, 65(1): 99–106.

Peters, R.; Dukai, B.; Vitalis, S.; van Liempt, J.; and Stoter, J. 2022. Automated 3D reconstruction of LoD2 and LoD1 models for all 10 million buildings of the Netherlands.

Poole, B.; Jain, A.; Barron, J. T.; and Mildenhall, B. 2022. Dreamfusion: Text-to-3d using 2d diffusion. *arXiv preprint arXiv:2209.14988*.

Ranftl, R.; Lasinger, K.; Hafner, D.; Schindler, K.; and Koltun, V. 2020. Towards robust monocular depth estimation: Mixing datasets for zero-shot cross-dataset transfer. *IEEE transactions on pattern analysis and machine intelligence*, 44(3): 1623–1637.

Richardson, E.; Metzer, G.; Alaluf, Y.; Giryes, R.; and Cohen-Or, D. 2023. Texture: Text-guided texturing of 3d shapes. In *ACM SIGGRAPH 2023 conference proceedings*, 1–11.

Rombach, R.; Blattmann, A.; Lorenz, D.; Esser, P.; and Ommer, B. 2022. High-Resolution Image Synthesis With Latent Diffusion Models. In *Proceedings of the IEEE/CVF Conference on Computer Vision and Pattern Recognition (CVPR)*, 10684–10695.

Saharia, C.; Ho, J.; Chan, W.; Salimans, T.; Fleet, D. J.; and Norouzi, M. 2022. Image super-resolution via iterative refinement. *IEEE transactions on pattern analysis and machine intelligence*, 45(4): 4713–4726.

SAVeNoW, P. 2020. LOD3 Road Space Models. <https://github.com/savenow/lod3-road-space-models>.

Song, Y.; Sohl-Dickstein, J.; Kingma, D. P.; Kumar, A.; Ermon, S.; and Poole, B. 2020. Score-based generative modeling through stochastic differential equations. *arXiv preprint arXiv:2011.13456*.

Sun, W.; Chen, S.; Liu, F.; Chen, Z.; Duan, Y.; Zhang, J.; and Wang, Y. 2024. Dimensionx: Create any 3d and 4d scenes from a single image with controllable video diffusion. *arXiv preprint arXiv:2411.04928*.

Wang, H.; Liu, Y.; Liu, Z.; Wang, W.; Dong, Z.; and Yang, B. 2024a. VistaDream: Sampling multiview consistent images for single-view scene reconstruction. *arXiv preprint arXiv:2410.16892*.

Wang, X.; Zhu, Z.; Huang, G.; Chen, X.; Zhu, J.; and Lu, J. 2024b. DriveDreamer: Towards Real-World-Drive World Models for Autonomous Driving. In *European Conference on Computer Vision*, 55–72. Springer.

Wang, Z.; Lu, C.; Wang, Y.; Bao, F.; Li, C.; Su, H.; and Zhu, J. 2023. Prolificdreamer: High-fidelity and diverse text-to-3d generation with variational score distillation. *Advances in Neural Information Processing Systems*, 36: 8406–8441.

Xie, H.; Chen, Z.; Hong, F.; and Liu, Z. 2024a. Citydreamer: Compositional generative model of unbounded 3d cities. In *Proceedings of the IEEE/CVF Conference on Computer Vision and Pattern Recognition*, 9666–9675.

Xie, H.; Chen, Z.; Hong, F.; and Liu, Z. 2024b. GaussianCity: Generative Gaussian Splatting for Unbounded 3D City Generation. *arXiv preprint arXiv:2406.06526*.

Xie, H.; Chen, Z.; Hong, F.; and Liu, Z. 2025. City-Dreamer4D: Compositional Generative Model of Unbounded 4D Cities. *arXiv:2501.08983*.

Yao, Z.; Chaturvedi, K.; and Kolbe, T. H. 2025. *3DCity-DBV5: Open Source 3D City Database for CityGML*. Chair of Geoinformatics, Technical University of Munich. Version 5.0, <https://www.3dcitydb.org/>.

Yu, H.-X.; Duan, H.; Herrmann, C.; Freeman, W. T.; and Wu, J. 2024a. WonderWorld: Interactive 3D Scene Generation from a Single Image. *arXiv preprint arXiv:2406.09394*.

Yu, H.-X.; Duan, H.; Hur, J.; Sargent, K.; Rubinstein, M.; Freeman, W. T.; Cole, F.; Sun, D.; Snavely, N.; Wu, J.; et al. 2024b. Wonderjourney: Going from anywhere to everywhere. In *Proceedings of the IEEE/CVF Conference on Computer Vision and Pattern Recognition*, 6658–6667.

Yu, W.; Xing, J.; Yuan, L.; Hu, W.; Li, X.; Huang, Z.; Gao, X.; Wong, T.-T.; Shan, Y.; and Tian, Y. 2024c. Viewcrafter: Taming video diffusion models for high-fidelity novel view synthesis. *arXiv preprint arXiv:2409.02048*.

Zhang, L.; Rao, A.; and Agrawala, M. 2023. Adding conditional control to text-to-image diffusion models. In *Proceedings of the IEEE/CVF international conference on computer vision*, 3836–3847.

Zhao, G.; Wang, X.; Zhu, Z.; Chen, X.; Huang, G.; Bao, X.; and Wang, X. 2024a. Drivedreamer-2: Llm-enhanced world models for diverse driving video generation. *arXiv preprint arXiv:2403.06845*.

Zhao, Y.; Zhou, Z.; Wang, Y.; Huang, J.; and Zhao, H. 2024b. EasySynth: A Unified Toolkit for Generating Multi-Modal Synthetic Data. <https://github.com/ydrive/EasySynth>. GitHub repository, accessed: 2025-08-01.

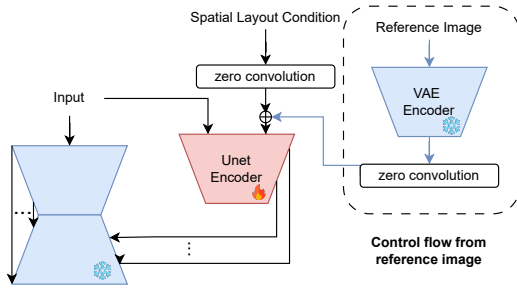


Figure 7: The architecture of ControlNet-N, the control flow from reference image gives extra condition to ControlNet

7 Data Preparation and Implementation

City Scene Data. Currently, there is a lack of publicly accessible high-quality datasets containing city mesh models that can provide sufficient rendering data for training a ControlNet. To evaluate the feasibility of our pipeline, we therefore leverage the detailed urban environment provided by the City Sample Project (Epic Games 2022) in Unreal Engine 5 (Epic Games 2021), which features two distinct cities with varied and realistic outdoor scenes. For training and evaluation purposes, we generate distinct camera sequences and render RGB images along with depth, normal, and semantic maps using modified versions of tools from MatrixCity (Li et al. 2023) and EasySynth (Zhao et al. 2024b). We set the rendering resolution to 960×544 with a field of view (FoV) of 45° , simulating the front camera of a vehicle to ensure good coverage of the forward view. The rendering interval is set at 1 meter, with the camera consistently facing forward horizontally. After this, we obtain $16k$ image with paired control signals for training the ControlNets.

Implementation Details. We utilize the training data described above to train two ControlNets (Zhang, Rao, and Agrawala 2023)—*ControlNet-S* and *ControlNet-N*—using the frozen *Stable Diffusion 1.5* (SD1.5) (Rombach et al. 2022) as the base model. Additionally for *ControlNet-N*, the extra control signal of warped image is randomly picked in the range of 10-20 meters ahead of the current view. Both networks are trained with a learning rate of $1e^{-5}$ and a batch size of 128 for $10k$ iterations. During scene generation, the next key frame is decided by thresholding the percentage of incompleteness to be outpainted, which roughly results into intervals of $\sim 20m$ distance with predefined threshold. For long-range generation, the sequence is divided into blocks, each consisting of 200 frames, which are processed through our pipeline. We employ an autoregressive approach for consistent generation, using the last generated frame from the previous block as the starting point for the next. We perform guided rectification on the latent for $N_g = 100$ iterations with a learning rate $lr = 0.00375$ at each timestep.

8 Trial on Mesh Texturing Method – Text2Tex

Several authors have attempted to adopt diffusion-based generative models (Ranftl et al. 2020; Bhat et al. 2023; Ke et al. 2024a; Saharia et al. 2022) to mesh texturing. TEXTure(Richardson et al. 2023) and Text2Tex(Chen et al. 2023a) utilize depth-to-image diffusion models to texture given meshes through inpainting. They tend to suffer from visible seams and a gradual amplification of texture artifacts. Another family of methods like Fantasia3D(Chen et al. 2023b), Decorate3D (Guo et al. 2023b), SceneTex(Chen et al. 2024) and Latent Paint(Metzer et al. 2023) is based on Score Distillation Sampling (SDS) (Poole et al. 2022; Wang et al. 2023), which is limited by the costly test-time optimization and restricted to single objects or indoor scenes with low polygon count. Moreover, these methods require coverage of the relevant view field with training views.

Text2Tex (Chen et al. 2024) is a method for mesh texturing based on depth-to-image generation models. It generates and inpaints visible mesh texel for each predefined camera views. At the end, a 3000×3000 RGB image is learnt to represent mesh texture of objects with UV mapping. We attempted to adopt it for outdoor scene mesh texturing. Unlike Objaverse(Deitke et al. 2023), instances from City Sample Project are high-poly meshes. To fit it into running code of Text2Tex, we simplify a city block of 100 meters via Quadric Edge Collapse Decimation(Garland and Heckbert 1997) and remove redundant parts except for visible mesh faces from camera views (the second column in Fig. 8). For the generation, We replace their inpainting diffusion module with ours, and extend the texture on the mesh surface by moving the camera backwards. Besides, we adopt a bigger size mesh texel with resolution 4096×4096 for better quality. After all, several random views are picked to further enhance the fidelity of the texture(Chen et al. 2024). As you can see in Fig. 8, there's apparent seams between each inpainted part. Restricted by its application only on small mesh models with low-poly, we could barely see its extendability on large scale egocentric video generation.

9 Implementation details of ControlNet-N

There is difference of processing the reference image compared to other control signals(depth, semantic and normal map). Similar to conditional latent diffusion model (Rombach et al. 2022), the reference image is at first processed by the VAE-Encoder and goes through several layers of convolution to align the feature dimension with other control signal features. We illustrate this in Fig. 7.

10 Distributing Flattened Gaussian Surfels On Mesh Surfaces

Our approach for surfel generation draws conceptual inspiration from WonderWorld (Yu et al. 2024a), where depth and surface normals are predicted for novel views. However, since we directly utilize mesh geometry, we bypass this prediction step by retrieving accurate depth and normal information through rasterization.

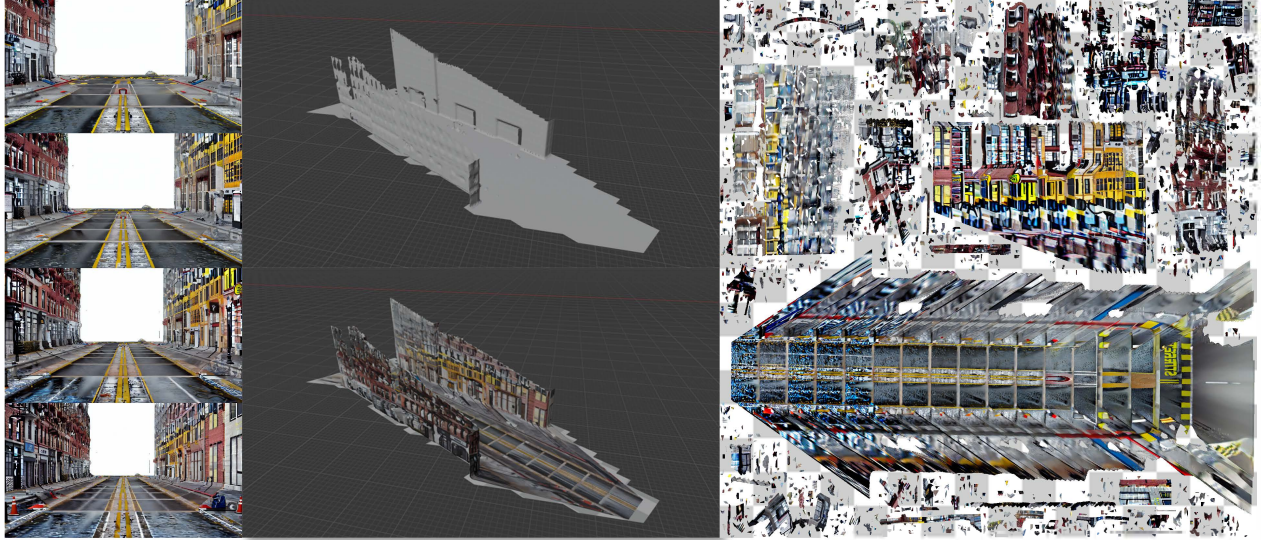


Figure 8: Crossroad Mesh Model for SceneTex Training

Here, Gaussian surfels are parameterized with position \mathbf{p} , orientation in quaternion form \mathbf{q} , scales in orthogonal directions $\mathbf{s} = [s_x, s_y, \epsilon]$, opacity o and RGB color \mathbf{c} . The Gaussian kernel at any spatial position \mathbf{x} is given by:

$$G(\mathbf{x}) = \exp\left(-\frac{1}{2}(\mathbf{x} - \mathbf{p})^T \Sigma^{-1}(\mathbf{x} - \mathbf{p})\right), \quad (4)$$

where the covariance matrix Σ encodes the shape and orientation of the surfel and is defined as:

$$\Sigma = \mathbf{Q} \cdot \text{diag}(s_x^2, s_y^2, \epsilon^2) \cdot \mathbf{Q}^T, \quad (5)$$

with \mathbf{Q} derived from the quaternion \mathbf{q} . Our rendering pipeline follows the same rasterization and alpha compositing process as the 3D Gaussian Splatting (3DGS) framework (Kerbl et al. 2023).

Given an image \mathbf{I} of resolution $H \times W$, we construct $H \times W$ Gaussian surfels. For each surfel, the position \mathbf{p} is directly derived from its corresponding 3D position on mesh, while it inherits color \mathbf{c} from the pixel's RGB value. We assume that all surfaces are Lambertian, so \mathbf{c} is treated as view-invariant. To avoid rendering artifacts such as undersampling or holes when zooming in, the scales along x and y axes are set as $d/\sqrt{2}f_x, d/\sqrt{2}f_y$, respectively. And ϵ is kept small enough but still larger than zero to avoid numerical errors. The opacity property is set to a constant 0.9. Similar to position, we align the surfel's normal with the mesh surface normal at the corresponding pixel. Then we receive the rotation matrix:

$$\mathbf{Q}_z = \mathbf{n}, \quad \mathbf{Q}_x = \frac{\mathbf{u} \times \mathbf{n}}{\|\mathbf{u} \times \mathbf{n}\|}, \quad \mathbf{Q}_y = \frac{\mathbf{n} \times \mathbf{Q}_x}{\|\mathbf{n} \times \mathbf{Q}_x\|}, \quad (6)$$

with the global up-direction $\mathbf{u} = [0, 1, 0]^T$ used to ensure a consistent coordinate frame.

11 Stylized Rendering

The following prompts are leveraged for the inference of Cosmos-Transfer1 (Alhaija et al. 2025) and TC-Light (Liu

et al. 2025) to achieve the visual results in the paper.

Full prompt for cosmos transfer1: A photorealistic scene of a quiet, empty urban street on a sunny day with some clouds in the sky. The wide road with yellow center lines stretches into the distance, flanked by tall buildings with classic architecture and street lamps. Some building fronts feature small potted shrubs, while a few windowsills display potted flowers or trailing leafy plants, adding touches of greenery and charm to the scene. The view is centered and symmetrical, creating a peaceful and cinematic atmosphere. Cool moonlight and warm streetlamp glows softly illuminate the buildings and pavement, casting gentle shadows. There are no people or vehicles, enhancing the stillness. Urban details like trash bins and cones add realism. The composition draws the eye toward a distant vanishing point.

Full prompt for TC-Light: A photorealistic depiction of a calm, empty urban street at noon on a sunny day.

We also include extra stylized videos in the attachment, they are generated by prompts:

Cosmos-transfer1 night time prompt: A photorealistic scene of a quiet, empty urban street at night under

a clear sky with scattered clouds. The wide road with yellow center lines stretches into the distance, flanked by tall buildings with classic architecture and street lamps. Some building fronts feature small potted shrubs, adding a touch of greenery to the scene. The view is centered and symmetrical, creating a peaceful and cinematic atmosphere. Cool moonlight and warm streetlamp glows softly illuminate the buildings and pavement, casting gentle shadows. Urban details like trash bins and cones add realism. The composition draws the eye toward a distant vanishing point.

TC-Light night time prompt: A photorealistic depiction of a calm, empty urban street at night under a moonlit sky.

Cosmos-transfer1 rainy day prompt: A photorealistic scene of a quiet, empty urban street during daytime under a cloudy, rainy sky. The wide road with yellow center lines stretches into the distance, flanked by tall buildings with classic architecture. Rows of street trees line both sides of the road, their wet trunks and leaves glistening slightly under the diffused daylight. The rain-slick asphalt reflects the buildings, trees, and urban elements, with scattered puddles creating mirror-like surfaces. Soft daylight filters through the overcast sky, producing muted shadows and emphasizing the textures of wet pavement and facades. Urban details like trash bins and traffic cones add realism. The composition is centered and symmetrical, guiding the eye toward a distant vanishing point softened by mist and rain.

Cosmos-transfer1 snowy day prompt: A photorealistic scene of a quiet, empty urban street during daytime in snowy weather. The wide road stretches into the distance, flanked by tall buildings with classic architecture and street lamps dusted with snow. Trees lining the sidewalks are covered with snow-laden branches, adding to the serene winter atmosphere. Some building fronts feature

small potted shrubs, adding subtle touches of greenery amid the white landscape. The view is centered and symmetrical, creating a peaceful and cinematic atmosphere. Soft daylight reflects off the snow-covered pavement and buildings, casting diffuse shadows. Urban details like trash bins and cones partially covered in snow add realism. The composition draws the eye toward a distant vanishing point.